Transverse and longitudinal magnons in the strongly anisotropic antiferromagnet $FePSe_3$

F. Le Mardelé,[1,*] A. El Mendili,[2] M. E. Zhitomirsky,[2,3] I. Mohelsky,[1] D. Jana,[1] I. Plutnarova,[4] Z. Sofer,[4] C. Faugeras,[1] M. Potemski,[1,5] and M. Orlita[1,6,†]

[1]*LNCMI-EMFL, CNRS UPR3228, Université Grenoble Alpes, Université Toulouse, Université Toulouse 3, INSA-T, Grenoble, France*

[2]*Université Grenoble Alpes, CEA, IRIG, PHELIQS, 38000 Grenoble, France*

[3]*Institut Laue-Langevin, 71 avenue des Martyrs, 38042 Grenoble, France*

[4]*Department of Inorganic Chemistry, University of Chemistry and Technology Prague, 16628 Prague, Czech Republic*

[5]*CENTERA Labs, Institute of High Pressure Physics, PAS, 01-142 Warsaw, Poland*

[6]*Institute of Physics, Charles University, Ke Karlovu 5, 12116 Prague, Czech Republic*

(Received 10 January 2024; revised 20 March 2024; accepted 20 March 2024; published 5 April 2024)

$FePSe_3$ is a collinear honeycomb antiferromagnet with an easy-axis anisotropy and large spins $S = 2$. It belongs to a family of magnetic van der Waals materials which recently attracted considerable attention. In this work we present an experimental magneto-optical study of the low-energy excitation spectrum in $FePSe_3$, together with its theoretical description. The observed response contains several types of magnon excitations. Two of them are conventional transverse magnons described by a classical theory of antiferromagnetic resonance. Two other modes are identified as multimagnon hexadecapole excitations with an anomalous g factor approximately equal to 4 times the g factor of a single Fe^{2+} ion. These quasiparticles correspond to full reversals of iron spins that coherently propagate in the up-down antiferromagnetic structure. They constitute a novel type of collective excitations in anisotropic magnetic solids, called longitudinal magnons. Comparison between theory and experiment allows us to estimate the microscopic parameters of $FePSe_3$, including exchange coupling constants and the single-ion anisotropy.

DOI: 10.1103/PhysRevB.109.134410

I. INTRODUCTION

$FePSe_3$ belongs to a family of transition-metal (M) chalcogen phosphates with the generic chemical formula MPX_3 (X = S, Se). These materials offer a unique test bed for studying quasi-two-dimensional ferromagnetic and antiferromagnetic structures in the insulating or metallic phase with bulk or few-layer samples down to the monolayer limit [1–3]. The electronic and magnetic properties of $FePSe_3$ are similar to those of the more studied sister compound $FePS_3$. Both materials are semiconductors with energy band gaps in the near-infrared range. Magnetic Fe^{2+} ions have a large spin $S = 2$ and form a honeycomb lattice in the ab plane [4–6]. Stacking of honeycomb layers follows the rhombohedral symmetry in $FePSe_3$, whereas in $FePS_3$ adjacent layers are slightly shifted in accordance with the monoclinic crystal structure [5]. Both materials order antiferromagnetically below comparable temperatures: $T_N = 118$ K ($FePS_3$) and $T_N = 106$ K ($FePSe_3$) [7]. In the ordered phases, their iron spins are oriented orthogonally to the ab layers and form ferromagnetic zigzag chains in the a direction that alternate antiferromagnetically along the b axis [8,9] (see Fig. 1).

The spin dynamics have been investigated in greater detail for $FePS_3$. Specifically, inelastic neutron-scattering measurements mapped the magnon dispersion in the entire Brillouin zone and provided us with values for the microscopic exchange interactions up to the third neighbors in the ab plane [10–12]. The magneto-optical response of $FePS_3$ in the ordered phase is dominated by an "acoustic" magnon with the gap $\Delta_1^s = 15.1$ meV visible in Raman and infrared experiments [13–18]. In a magnetic field, this mode splits into two branches linear in B, with $S^z = \pm 1$ and a gyromagnetic factor of $g \approx 2.15$. Thus, $FePS_3$ provides a textbook example of antiferromagnetic resonance (AFMR) in an easy-axis antiferromagnet [19–21].

The recent magneto-optical experiments on $FePSe_3$ found a new appealing effect in this material in comparison to $FePS_3$. The lowest antiferromagnetic ("acoustic") magnon located at $\Delta_1^s \simeq 14.4$ meV interacts with a pair of quasidegenerate chiral phonons [22,23]. The chirality selective hybridization couples the phonon angular momentum to the magnon dipole moment. Interestingly, this coupling was observed on $FePSe_3$ samples, using the polarization-resolved magneto-Raman scattering technique, down to a monolayer limit [22].

The magnetic excitation spectrum of $FePS_3$ exhibits an unusual richness at high energies [18]. Apart from the acoustic magnon, there is an "optical" magnon mode with $\Delta_1^a = 39.6$ meV and the same g factor. The presence of two pairs of $k = 0$ magnons is a direct consequence of the four-sublattice antiferromagnetic structure. The corresponding gaps are in good agreement with the neutron-scattering experiments [11,12]. Still, at higher energies, there is an extra

*florian.le-mardele@lncmi.cnrs.fr
†milan.orlita@lncmi.cnrs.fr

 ©2024 American Physical Society

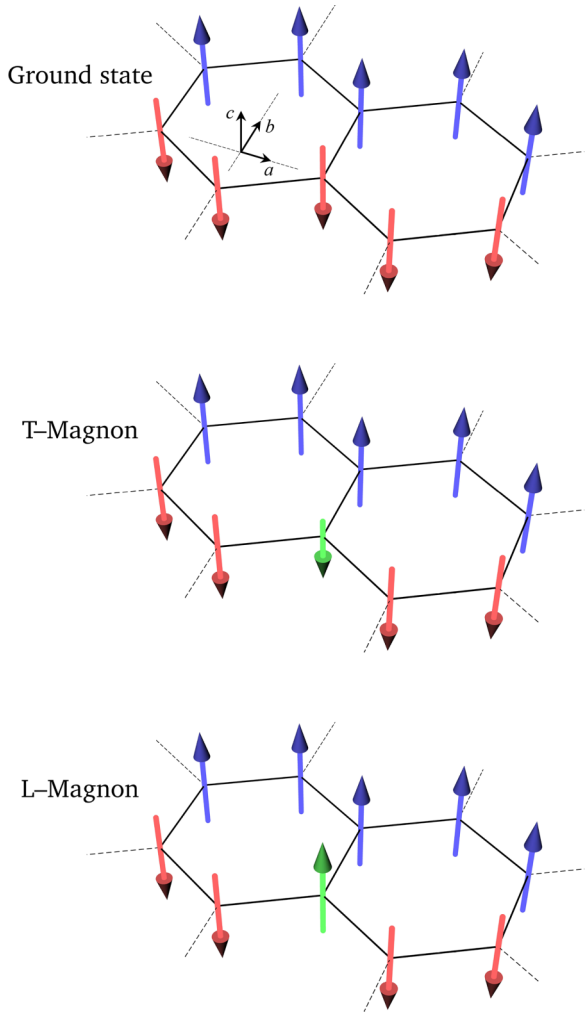

FIG. 1. Cartoon representation of T- and L-magnons localized on a single lattice site (green arrow). Top: a collinear zigzag antiferromagnetic structure in $FePSe_3$ and $FePS_3$ materials. Middle: an ordinary transverse magnon, or T-magnon, with $|\Delta S^z| = 1$. Bottom: a longitudinal magnon, or L-magnon, with $|\Delta S^z| = 2S$ ($= 4$ for $S = 2$ of Fe^{2+} ions).

line at $\Delta_4 = 57.5$ meV, which splits in magnetic field with a large effective g factor: $g_4 \approx 4g$. This specific magnetic mode was interpreted [18] in terms of a full reversal of an iron spin. Such an excitation carries a large angular momentum, $|S^z| = 2S = 4$, and can be called a longitudinal (L) magnon in order to distinguish it from conventional transverse (T) magnons with $|S^z| = 1$, corresponding to transverse precession of coupled magnetic dipoles.

Similar excitations were theoretically discussed for spin-1 easy-axis ferro- and antiferromagnets [24,25] and experimentally observed in FeI_2 with effective $S = 1$ [26–28]. For $S = 1$, the angular momentum of an excitation with a reversed spin is $|S^z| = 2$; hence, it was called a single-ion two-magnon bound state [24]. For $FePS_3$ with $S = 2$, the L-magnon can be optionally called a single-ion four-magnon bound state. In order to distinguish this type of excitation from the exchange-driven multimagnon states observed in recent experiments [29,30], we use the term "L-magnon" (see also Sec. II).

In this paper, we report on the infrared magnetospectroscopy study of $FePSe_3$ in a broader frequency range compared to that in previous works on this material [22,23,31]. Like for $FePS_3$, we find an optical magnon at $\Delta_1^a \approx 35$ meV. In addition, we observe *two pairs* of L-magnons with energies $\Delta_4^s \approx 53$ meV and $\Delta_4^a \approx 55$ meV. The presence of two pairs of L-magnons implies that these excitations have a sizable dispersion in the Brillouin zone rather than being completely localized on the same site as the classical excitations in Ising models do. Thus, we extend and strengthen the previous observation of L-magnons with $S^z = 4$ in $FePS_3$ [18] by demonstrating their collective nature and firmly establishing them as a novel type of quantum quasiparticle.

This paper is organized as follows. Section II provides a general theoretical description of L-magnons. The obtained experimental results are described in Sec. III. By comparing theory and experiment for two pairs of T- and L-magnons, we are able to extract the microscopic parameters of $FePSe_3$, which may stimulate future neutron-scattering studies of this material.

II. THEORY

A. Transverse magnons

The two-dimensional spin Hamiltonian for layered $FePX_3$ ($X = $ S, Se) materials with easy-axis anisotropy can be written as [11,18]

$$\hat{\mathcal{H}} = \sum_{\langle ij \rangle} J_{ij} \mathbf{S}_i \cdot \mathbf{S}_j - D \sum_i S_i^{z2} - g\mu_B B \sum_i S_i^z. \qquad (1)$$

Here, $\mathbf{S}_i$ are $S = 2$ operators residing on a honeycomb lattice. Exchange interactions J_{ij} up to the third neighbors are necessary to include in order to describe the zigzag antiferromagnetic structure [32,33]. We neglect magnetic coupling between planes, which is 2 orders of magnitude weaker than the largest in-plane exchange coupling [11,34]. On the other hand, the single-ion constant D is comparable to the in-plane exchanges producing pronounced magnetic anisotropy in the magnetization of $FePS_3$ [33] and large excitation gaps.

In collinear antiferromagnets, magnons are coherently propagating spin flips with $S^z = \pm 1$ (see Fig. 1). At the semiclassical level, such excitations can be viewed as the transverse precession of coupled magnetic dipoles. The standard spin-wave theory based on the Holstein-Primakoff representation of spin operators is commonly used to compute the magnon dispersion. The full expressions for magnon bands in $FePX_3$ are given, for example, by Wildes *et al.* [10]. Below we provide only the energies of the $k = 0$ magnons that are directly measured in the magneto-optical experiments. For the up-up-down-down magnetic structure of $FePX_3$, the spectrum consists of two pairs of T-magnons corresponding to symmetric (s) and antisymmetric (a) oscillations of parallel spins in ferromagnetic zigzag chains:

$$\Delta_1^s = 2S\sqrt{\bar{D}(\bar{D} + J_1 + 4J_2 + 3J_3)} \pm g\mu_B B \qquad (2)$$

and

$$\Delta_1^a = 2S\sqrt{(\bar{D} - 2J_1 + 4J_2)(\bar{D} - J_1 + 3J_3)} \pm g\mu_B B. \qquad (3)$$

In these expressions we have included a renormalized constant $\bar{D} = D[1 - 1/(2S)]$ [35–37], which merely reflects the fact that a single-ion anisotropy is mute for $S = 1/2$. Formally, this quantum correction corresponds to the next order in the $1/S$ expansion and is often neglected in the linear spin-wave fits of the experimental data, but see [38] for an exception. As a result, the bare single-ion anisotropy constant deduced, e.g., from the AFMR measurements is underestimated, for $S = 2$ by ∼30%. In the following theoretical description of L-magnons, one has to employ a bare parameter D. For that we straightforwardly modify the previously reported anisotropy values to include this correction.

B. Longitudinal magnons

Two-magnon bound states appear due to the attraction between spin flips on adjacent sites in ferromagnets [39,40] as well as in materials with mixed ferro- and antiferromagnetic bonds [41]. Multi-magnon bond states consisting of n > 2 spin flips may also appear due to the exchange attraction mechanism, though dimensionality and frustration are crucial in that case [42]. Alternatively, for $S > 1/2$, a single-ion anisotropy of the easy-axis sign induces attraction for spin flips on the same site [24]. It is energetically favorable to bring together as many spin flips as allowed by the spin quantum number S. The corresponding $2S$-magnon bound states can emerge without the presence of bound states in the lower-magnon subsectors. Because of this and in order to avoid an unnecessary dependence of the terminology on the quantum spin value, we call them longitudinal magnons, or L-magnons, as opposed to ordinary transverse magnons, or T-magnons. Longitudinal magnons may appear as a distinct type of magnetic excitation in materials with strong easy-axis anisotropy. As anisotropy weakens, the L-magnon band starts to overlap with the $2S$-magnon continuum and acquires a finite lifetime due to magnon-magnon interaction.

A convenient starting point for a theoretical description of L-magnons is the large-D limit, $D \gg J_{ij}$. A local excitation $|\pm S\rangle \to |\mp S\rangle$ acquires energy from broken exchange bonds with adjacent spins but leaves unchanged the single-ion term. Keeping a full spin flip completely localized, one can easily compute its energy [18,27]. For the zigzag antiferromagnetic structure of $FePX_3$ materials this yields

$$\Delta_4 = 2S^2(-J_1 + 2J_2 + 3J_3) \pm 4g\mu_B B. \tag{4}$$

In this "Ising" approximation, the energy of L-magnons has no k dependence, and the excitations remain completely localized. The dispersion of L-magnons and hence their collective nature are recovered by performing an expansion in powers of J_{ij}/D. Specifically, we associate two degenerate states $(|+S\rangle, |-S\rangle)_i$ on every site with a pseudo-spin-1/2 doublet $(|\uparrow\rangle, |\downarrow\rangle)_i$ and consider separately the expansion for each exchange bond. For general spins $S > 1/2$, one has to resort to at least the $2S$ order to realize a flip $|\pm S\rangle \to |\mp S\rangle$. This results in the effective bond Hamiltonian:

$$\hat{\mathcal{H}}_n^{\text{eff}} = \tilde{J}_n^{\perp}\left(s_i^x s_j^x + s_i^y s_j^y\right) + \tilde{J}_n^z s_i^z s_j^z + \text{const}, \tag{5}$$

where s_i^α are spin-1/2 operators.

For $FePX_3$ materials with $S = 2$, the transverse and Ising constants in Eq. (5) are expressed as

$$\tilde{J}_n^{\perp} = -\frac{J_n^4}{4D^3} + \frac{3J_n^5}{8D^4}, \quad \tilde{J}_n^z = 16J_n + \frac{4J_n^2}{3D}. \tag{6}$$

Here, we include two leading contributions for each $\tilde{J}_n$ from an infinite series in powers of J_n/D. The higher orders additionally generate multisite terms in the effective Hamiltonian.

An L-magnon corresponds to a flip of a pseudospin $|\uparrow\rangle \to |\downarrow\rangle$. The Ising interactions between pseudospins reproduce expression (4) in the leading order, whereas transverse terms are responsible for the L-magnon dispersion. The L-magnon bandwidth is obviously small in comparison to that of the ordinary magnons but still non-negligible. The full dispersion of L-magnons can be obtained by performing the harmonic spin-wave calculation for the effective spin-1/2 Hamiltonian combining all bond contributions (5). As a result, we obtain two doubly degenerate branches:

$$E_{\mathbf{k}}^{\pm 2} = \tfrac{1}{4}\left(A^2 + |B_0|^2 - B_1^2 - |B_2|^2\right) \pm \tfrac{1}{2}\sqrt{|AB_0 - B_1B_2|^2 - [\text{Im}(B_0B_2^*)]^2}, \tag{7}$$

with

$$\begin{aligned} A &= 3\tilde{J}_3^z - \tilde{J}_1^z + 2\left[\tilde{J}_2^z + \tilde{J}_2^{\perp}\,\text{Re}\,(\gamma_1\gamma_3^*)\right], \\ B_0 &= (\gamma_1 + \gamma_3)\tilde{J}_1^{\perp}, \quad B_1 = \text{Re}[\gamma_2^*(\gamma_1 + \gamma_3)]\tilde{J}_2^{\perp}, \\ B_2 &= \gamma_2\tilde{J}_1^{\perp} + \left(\gamma_1^{*2} + \gamma_2^{*2} + \gamma_3^{*2}\right)\tilde{J}_3^{\perp}, \\ \gamma_1 &= e^{ik_x}, \quad \gamma_2 = e^{i(-k_x + \sqrt{3}k_y)/2}, \quad \gamma_3 = e^{-i(k_x + \sqrt{3}k_y)/2}. \end{aligned} \tag{8}$$

An illustration of this dispersion is presented below in Fig. 5 using microscopic parameters extracted later on from the experimental data for $FePSe_3$. Interestingly, the L-magnons have almost quasi-one-dimensional bands with a strongly dispersive direction parallel to the ferromagnetic chains of the zigzag structure. This property follows naturally from small $\tilde{J}_n^{\perp} \ll \tilde{J}_n^z$.

The energy gaps for the symmetric and antisymmetric L-magnons with $k = 0$ measured in the optical experiments are expressed as

$$\Delta_4^{s,a} = \Delta_4 - \frac{2J_1^2 - 4J_2^2 - 6J_3^2}{3D} + \tilde{J}_2^{\perp} \mp |\tilde{J}_1^{\perp}|, \tag{9}$$

where Δ_4 is given by Eq. (4) with $S = 2$. The above expression is based on the strong-coupling expansion, which generally loses its accuracy for $J_n \sim D$. Still, from a comparison of the first two contributions to the effective interaction parameters (6) we can conclude that the "center-of-mass" position of two modes $(\Delta_4^s + \Delta_4^a)/2$ is given by Eq. (9) with a higher accuracy compared to the gap splitting $(\Delta_4^a - \Delta_4^s)$.

In $FePS_3$, the lower L-magnon mode is found at $\Delta_4^s \approx 57.5$ meV and thus lies outside the four-magnon continuum, which starts at $4\Delta_1^s = 60.4$ meV [18] (see Table I). The upper L-magnon mode Δ_4^a is nearly vanishing. Most likely, this mode merges with the onset of the four-magnon continuum and therefore decays quickly due to magnon-magnon interaction. We have used the set of microscopic parameters provided for $FePS_3$ in [12] (Table II) to estimate from Eq. (9) the gap splitting as $\Delta_4^a - \Delta_4^s \approx 2.4$ meV. This value is sufficient to

TABLE I. Energies of selected magnon modes observed in $FePSe_3$ extracted from our magnetotransmission data (Figs. 2 and 3) compared to analogous modes active in the response of $FePS_3$. The latter parameters are taken from Ref. [12] and were used to reproduce the L-magnon mode in the preceding study of $FePS_3$ by Wyzula *et al.* [18]. All values are in meV.

	$FePSe_3$		$FePS_3$	
Magnon mode	Energy (meV)	g factor	Energy (meV)	g factor
M_1^s	14.5	2.1	15.1	2.15
M_1^a	34.6	2.1	39.6	2.15
M_β	48.8	6.9	54.0	5.0
M_4^s	52.6	8.9	57.5	9.2
M_4^a	55.0	7.8	60.6	7.3

make Δ_4^a approach the four-magnon continuum boundary and thus may explain its weak intensity.

III. EXPERIMENTAL RESULTS

$FePSe_3$ was prepared by chemical vapor transport from elements in a quartz glass ampoule. Iron (3N, 5–9 μm, Strem, Germany) phosphorus (6N, 2–6 mm granules, Wuhan Xinrong New Material Co., China), and selenium (6N, 2–6 mm granules, Wuhan Xinrong New Material Co., China) were placed in an ampoule corresponding to 20 g of $FePSe_3$. Iodine was used as a transport medium (0.4 g, 3N, 1–3 mm, Fisher Scientific, United States) together with 1 at % excess of selenium and phosphorus. The elements were sealed in a quartz ampoule under high vacuum (1×10^{-3} Pa, diffusion pump with a liquid nitrogen trap) using an oxygen-hydrogen torch. The ampoule was first placed in a muffle furnace to cause the elements to react and form bulk $FePSe_3$. The ampoule was heated first to 450 °C for 25 h and subsequently to 500 °C for 50 h and to 600 °C for 50 h. The heating rate was 0.2 °C/min, and the cooling rate was 1 °C/min. The ampoule with bulk $FePSe_3$ was placed in a two-zone furnace, and first, the growth zone was heated to 700 °C, while the source zone was kept at 500 °C. After 50 h the thermal gradient was reversed, and the source zone was heated to 700 °C, while the growth zone temperature was decreased from 650 to 600 °C over a period of 5 days and for the following 5 days was kept at 600 °C. Finally, during the cooling procedure the growth zone was kept at 300 °C for 2 h to remove all transport media from the growth zone. The ampoule was opened in an argon-filled glove box.

TABLE II. Microscopic parameters of $FePSe_3$ deduced from the magneto-optical measurements. Similar parameters obtained for $FePS_3$ [12] are listed for comparison. All values are given in meV.

	$FePSe_3$	$FePS_3$
J_1	-2.5 ± 0.2	-2.92
J_2	0.5 ± 1.0	0.44
J_3	1.0 ± 0.7	1.1
$\bar{D}$	2.8 ± 0.9	2.46
D	3.7 ± 1.2	3.28

The magneto-optical response of $FePSe_3$ was probed in the transmission mode and in the Faraday configuration, with the magnetic field perpendicular to the sample surface (along the c axis). The radiation from a mercury lamp, or, alternatively, a globar, was analyzed by a Bruker Vertex 80v Fourier-transform spectrometer and delivered to the sample via light-pipe optics. The $FePSe_3$ sample (with an effective irradiated area of several square millimeters and a thickness of ≈100 μm) was kept at $T = 4.2$ K in the helium exchange gas. In experiments using a superconducting coil (below 16 T), the radiation was detected by a composite bolometer placed right below the sample. When working with the resistive coil (above 16 T), to avoid excessive noise generated by the cooling water, the sample was placed on a mirror and probed in the so-called double-pass transmission mode. The radiation was then detected by an external bolometer. The latter configuration is possible thanks to the insulating nature of the sample, thus remaining highly transparent at low photon energies (apart from several phonon modes).

The collected magnetotransmission data are plotted in Figs. 2 and 3. In the three selected spectral ranges, five distinct magnon-type excitations are identified. A remarkable similarity is found between the responses of $FePSe_3$ and $FePS_3$, which greatly facilitates the interpretation of individual modes. To be consistent with Ref. [18], we label these modes M_1^s, M_1^a, M_β, M_4^s, and M_4^a in order, respecting the energy of transitions. The corresponding zero-field energies are Δ_1^s, Δ_1^a, Δ_β, Δ_4^s, and Δ_4^a, respectively. The deduced energies are summarized in Table I and compared to those found in $FePS_3$. We now proceed with a more in-depth analysis.

We start with the two most pronounced modes M_1^s and M_1^a, having energies $\Delta_1^s = (14.5 \pm 0.5)$ meV and $\Delta_1^a = (34.6 \pm 0.2)$ meV, respectively. These two modes are conventional one-magnon gaps, or, using the above-introduced terminology, T-magnon modes. The upper optical mode M_1^a follows the classical Kittel formula for the AFMR [19]: $\Delta_1^a(B) = \Delta_1^a \pm g_1 \mu_B B$, where the effective g factor reaches 2.1. The same characteristic behavior is observed for the acoustic mode M_1^s at higher magnetic fields (above 10 T).

The M_1^s mode exhibits, at low magnetic fields, a distinctively different behavior from the classical AFMR. This is due to a pronounced magnon-phonon (magnon-polaron) coupling, which was already observed in previous infrared and Raman magnetospectroscopy studies of $FePSe_3$ [22,23,31]. This coupling was also found in the sister compound $FePS_3$ [16,17,34,43], where the lower one-magnon gap has a nearly identical energy. To estimate the bare energy of Δ_1^s, free of magnon-phonon coupling, we extrapolated the high-field part of the data using Kittel's formula [19].

Two other very visible modes, M_4^s and M_4^a, appear at higher photon energies in the midinfrared spectral range: $\Delta_4^s = (52.5 \pm 0.5)$ meV and $\Delta_4^a = (55.0 \pm 0.5)$ meV. At first glance, they also resemble the classical AFMR response—both modes split symmetrically into two branches that are linear in B. However, a closer inspection reveals that the effective g_4 factor is roughly 4 times larger than g_1. These transitions may be interpreted in terms of a single-ion four-magnon bound state, i.e., L-magnon modes in an $S = 2$

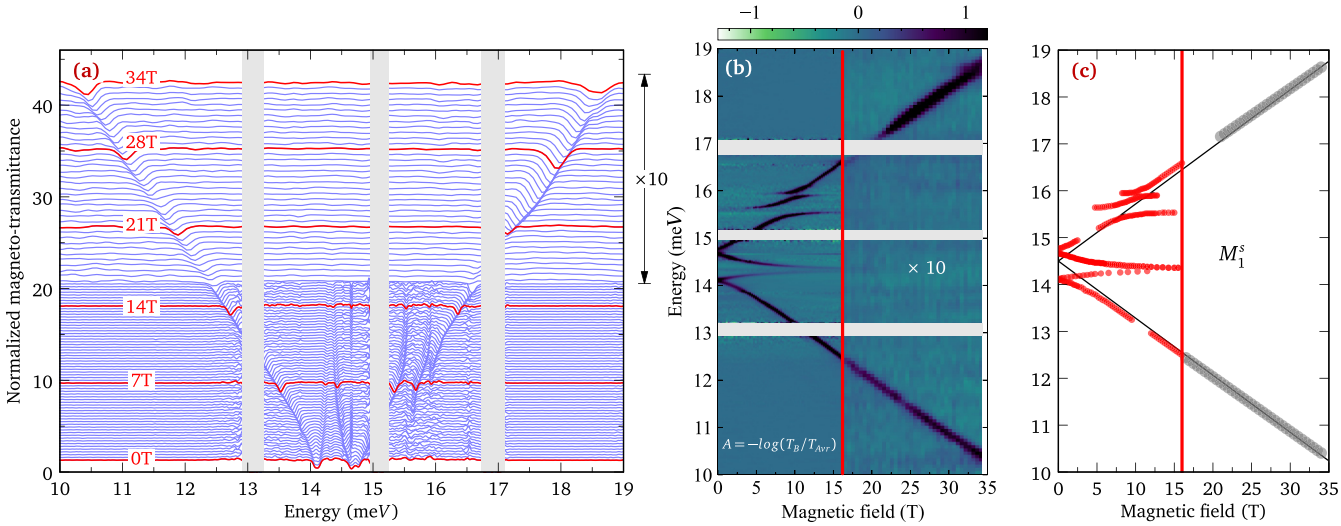

FIG. 2. Magnetotransmission data collected on $FePSe_3$ in the THz range at $T = 4.2$ K plotted in the form of (a) a stack plot and (b) a false-color map. Two distinct sets of data are plotted, collected in the superconducting and resistive coils, below and above 16 T, respectively. Each magnetotransmission spectrum is normalized by the transmission averaged over the explored range (0–16 and 0–34 T). The gray areas correspond to the region of full opacity due to optical phonon modes. (c) The extracted magnetotransmission minima. Only the high-field part of the data (gray solid circles) was used to fit (solid lines) the Δ_1^s energy and the corresponding g factor (Table I).

system. Such an excitation, at almost the same photon energy, was also recently identified in $FePS_3$ [18]. Similar to that in $FePS_3$, the L-magnon in $FePSe_3$ is a weak excitation, with the integral strength being a factor of 10^3 smaller compared to that of the M_1^s mode.

The remaining magnon-type mode, M_β, is a very weak excitation. It seems to be another multimagnon mode. In this particular case, however, we may only speculate about its origin. Again, a similar line was also revealed in the response of $FePS_3$ and was interpreted as a three-magnon bound state. The extracted effective g factor $g_\beta = 6.9$ supports such a view.

The similarity between the magneto-optical responses of $FePS_3$ and of $FePSe_3$ greatly facilitated the interpretation of magnonlike excitations observed in the latter material (compare Figs. 2 and 3 with [18]). This similarity concerns the energies, effective g factors, and the relative strengths of individual modes. All this suggests that the theoretical model for magnon excitations in $FePS_3$—invoked in Ref. [18] and extended in Sec. II—is also relevant to $FePSe_3$.

Since the energy separation of the observed longitudinal modes is relatively small ($\Delta_4^a - \Delta_4^s \approx 2.4$ meV) and our theory (9) describes this splitting only perturbatively, let us put it aside for a while. Instead, we assume that $(\Delta_4^s + \Delta_4^a)/2 \approx \Delta_4^a \approx \Delta_4^s \approx 54$ meV. This allows us to use Eqs. (2) and (3), together with the center of mass in (9), i.e., with $\tilde{J}_1^\perp = 0$, to estimate the exchange coupling constants and the single-ion magnetic anisotropy in $FePSe_3$ based on the experimentally determined energies of magnon modes, a piece of information still missing in the literature.

The zero-field energies of magnon excitations, (2), (3), and (9), represent a set of three equations for four unknown parameters: J_n for $n = 1$–3 and $\bar{D}$. To proceed with such an underdetermined problem, we choose to parametrize it in $\bar{D}$ and search for additional constraints, such as the experimentally established magnetic structure of $FePSe_3$ in zero field [8]. Clearly, the characteristic zigzag chains do not emerge for arbitrary combinations of the parameters.

This is shown in Fig. 4(a), where we plot the phase diagram established in [33]. This diagram was obtained considering a reduced Ising-type Hamiltonian with out-of-plane $S = 2$ spins organized in a honeycomb lattice. Such an approach is applicable in the case of a relatively strong easy-axis anisotropy, i.e., $D \gtrsim \max|J_n|$ for $n = 1$–3. This assumption is justified *a posteriori*. The red curve in Fig. 4(a) is a result of our parametrization, showing the ratios of the exchange constants as a function of $\bar{D}$. We infer that the antiferromagnetic zigzag arrangement of spins is possible for only certain values of the magnetic anisotropy: $1.9 < \bar{D}(\text{meV}) < 3.6$. If $\bar{D}$ is too large, a ferromagnetic phase emerges. If $\bar{D}$ is too small, no real solution exists.

Values of the exchange constants J_1, J_2, and J_3 evaluated as a function of the (renormalized) single-ion parameter $\bar{D}$ are plotted in Fig. 4(b) and listed in Table II. In the relevant interval of $\bar{D} = (2.8 \pm 0.9)$ meV, the nearest-neighbor coupling J_1 remains nearly constant, allowing us to set its value as $J_1 = -(2.5 \pm 0.2)$ meV. The other two exchange constants evolve considerably with $\bar{D}$. This leaves us with relatively large uncertainties of their values: $J_2 = (0.5 \pm 1.0)$ meV and $J_3 = (1.0 \pm 0.7)$ meV. Nevertheless, the simplified Eq. (4) for the L-magnon energy does not depend on $\bar{D}$. This allows us, after establishing the value of J_1, to find a simple approximate relation in the leading order: $2J_2 + 3J_3 \approx 4.2$ meV, which helps us to reduce the uncertainty in the J_2 and J_3 parameters.

It is instructive to compare the values of the exchange constants estimated for $FePSe_3$ with those already known for the sibling compound $FePS_3$. At present, there are several sets of parameters proposed for the latter material [11,44,45]. In Fig. 4(b), the color-coded solid circles show the values of J_n at the corresponding single-ion magnetic anisotropy $\bar{D} = 2.46$ meV. These values were recently suggested in

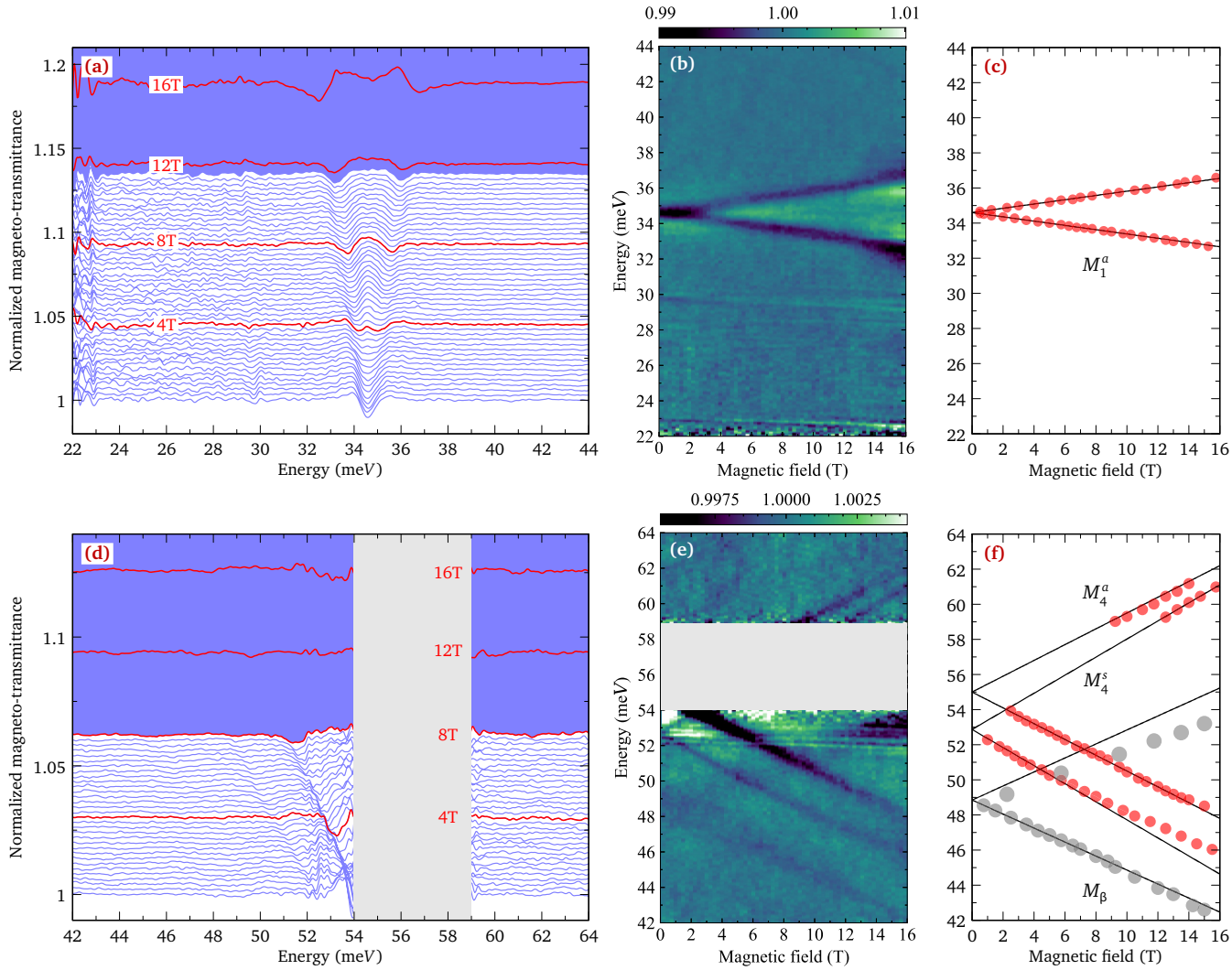

FIG. 3. Magnetotransmission data collected on $FePSe_3$ at $T = 4.2$ K in two midinfrared spectral ranges plotted in the form of (a) and (d) stack plots and (b) and (e) false-color maps in the magnetic field up to 16 T. In both cases, the magnetotransmission spectra are normalized by the transmission spectrum averaged over an interval of 10 T centered at B. The gray areas correspond to the region of full opacity due to optical phonon modes. (c) and (f) The extracted magnetotransmission minima. The solid lines are fitted using the classical Kittel formula, yielding the zero-field energies of Δ_β, Δ_4^s, and Δ_4^a and the corresponding effective g factors (Table I).

Ref. [12], where the magnon dispersion obtained in the neutron-scattering experiments was fitted using the extended version of the spin Hamiltonian (1), which includes a biquadratic exchange. Notably, these values lead to the correct estimate of the four-magnon energy (4) in $FePS_3$ and are only slightly different from those extracted here for $FePSe_3$. Both sets are compared in Table II.

Let us now return to the observed splitting of the longitudinal mode ($\Delta_4^s \neq \Delta_4^a$). According to Eq. (9), two $k = 0$ branches, the symmetric and antisymmetric ones, are expected to appear for the L-magnon mode due to the four-sublattice structure of $FePSe_3$, separated by an energy of $2|\tilde{J}_1^\perp|$. Using Eq. (6) and the above evaluated intervals for J_1 and $\bar{D}$, we obtain the splitting $\Delta_4^a - \Delta_4^s \in (0.2\text{–}7.7)$ meV. The experimentally observed value of 2.4 meV lies within this interval, thus corroborating our overall data interpretation. Let us also note that the two L-magnon modes identified in $FePSe_3$ display slightly different effective g factors (see Table I). This difference suggests some additional spin-orbit effects not accounted for in our simplified theoretical approach in Sec. II.

Figure 5 illustrates the in-plane dispersion of the L-magnon with both the symmetric and antisymmetric branches, which give rise to two optically active $k = 0$ modes. As mentioned above, the plotted dispersion has almost a one-dimensional character, displaying a strongly dispersive direction parallel to the ferromagnetic chains of the zigzag structure. The dispersion was computed for the following set of parameters: $J_1 = -2.47$ meV, $J_2 = 1.39$ meV, $J_3 = 0.5$ meV, and $\bar{D} = 1.99$ meV. These values were obtained by using the full Eq. (9) together with T-magnon energies from Eqs. (2) and (3). In such a case, we conveniently solve four independent equations and obtain four parameters as a result. Nevertheless, let us mention again that the splitting of the L-magnon modes

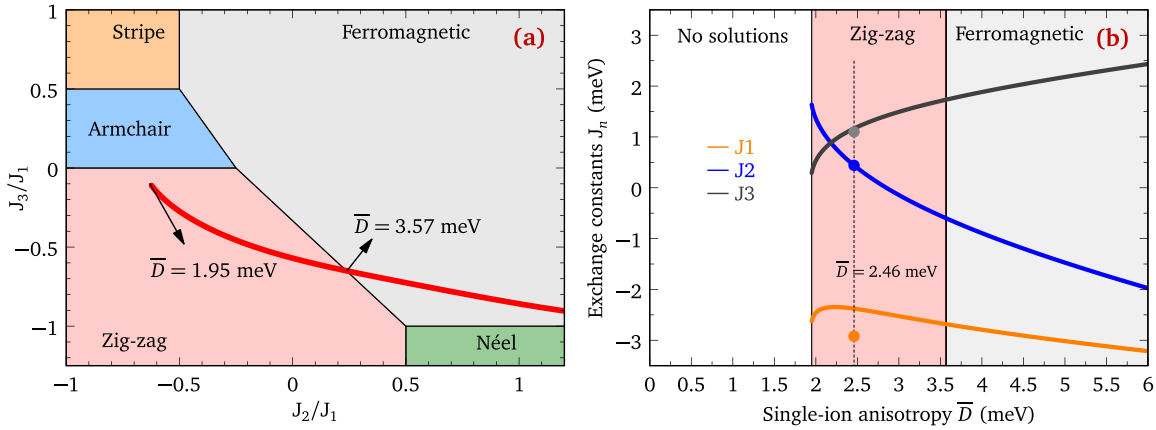

FIG. 4. (a) Phase diagram of the J_1-J_2-J_3 honeycomb antiferromagnet with strong easy-axis anisotropy (see main text and Ref. [33]). The red curve represents solutions of Eqs. (2)–(4) parametrized using the single-ion constant $\overline{D}$. No solution exists for $\overline{D} < 1.9$ meV. The zigzag antiferromagnetic structure appears only for $1.9 < \overline{D}(\text{meV}) < 3.6$. (b) Exchange coupling constant values J_n for $n = 1$–3 corresponding to the experimental gaps as a function of the anisotropy parameter $\overline{D}$. Solid circles in (b) show values of exchange constants in $FePS_3$ consistent with the L-magnon gap in this material [18].

in Eq. (9) has a lower accuracy than their mean (center-of-mass) energy and the exchange constants listed in Table II.

Finding this theoretically anticipated splitting in the experimental data serves as an indication that the observed four-magnon line does not correspond to a localized state in the magnetic lattice, but, instead, to a dispersing quantum quasiparticle. This finding also allows us to reinterpret the weak magnonlike mode M_α observed in our previous study of $FePS_3$ (see the supplementary materials of Ref. [18]), which now appears to be the antisymmetric branch of the L-magnon M_4^a. This mode overlaps with the onset of the four-magnon continuum, which explains its integral intensity, which is significantly weaker than M_4^s in $FePS_3$.

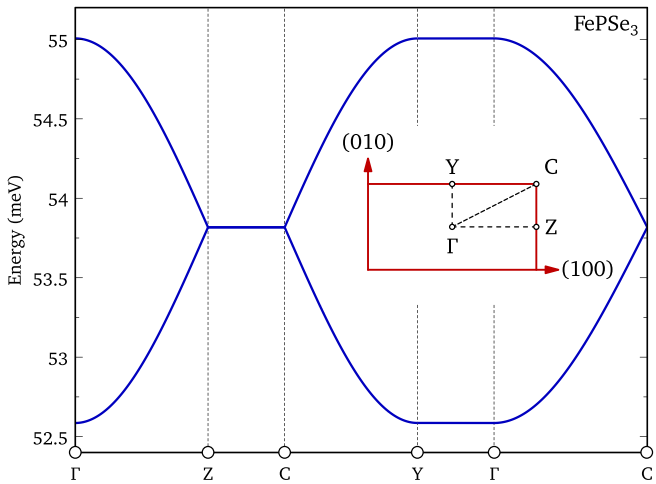

FIG. 5. Computed dispersion of longitudinal magnons using the microscopic parameters of $FePSe_3$ listed in Table II. The inset specifies the chosen path in the Brillouin zone. The most and least dispersive sections of the path correspond to parallel and orthogonal directions with respect to the ferromagnetic zigzag chains, which are, in turn, parallel to the crystallographic a axis.

IV. CONCLUSIONS

We measured magneto-optically active excitations in $FePSe_3$ in the infrared spectral range. The excitation spectrum is composed of conventional transverse magnons with $|S^z| = 1$ and longitudinal magnons with $|S^z| = 4$. The latter can be viewed as $2S$-magnon single-ion bound states brought up by a strong easy-axis anisotropy. The magneto-optical activity of these high angular momentum excitations signifies their mixed dipole-hexadecapole symmetry. Such a mixing may be induced by higher-order terms in the crystal-field Hamiltonian present due to the local C_3 rotation symmetry on magnetic sites of a honeycomb lattice or by other spin-orbital effects. In contrast to the previously studied $FePS_3$ [18], we observed two split pairs of L-magnons that correspond to symmetric and antisymmetric oscillations in the magnetic unit cell, which contains four Fe^{2+} ions. The strong-coupling expansion ($D \gg J_{ij}$) was used to theoretically compute the observed splitting and the overall dispersion of the L-magnon band. The investigation of the intermediate regime ($J_{ij} \sim D$), including L-magnon decay, is a subject of interest for our future work.

Comparing the theoretical results with the experimental data allowed us to estimate the exchange parameters and the magnetic anisotropy constant for $FePSe_3$. It will be interesting to directly measure the L-magnon excitations together with their dispersion in inelastic neutron-scattering experiments. This would establish longitudinal magnons as a novel type of collective magnetic excitations in strongly anisotropic magnetic solids. Finally, a finite bandwidth (∼2.4 meV) of the longitudinal magnons suggests that the condensation of these $|S^z| = 4$ quasiparticles at strong magnetic fields may result in a new quantum hexadecapole state stable in a few-tesla range in the vicinity of the condensation field. Such a possibility calls for high magnetic field measurements on $FePSe_3$ similar to the study performed on the sister material $FePS_3$ [33].

Note added in proof. The values of exchange constants and magnetic anisotropy, similar to those derived in our study, have recently been determined from neutron scattering experiments on $FePSe_3$ [46].

ACKNOWLEDGMENTS

We thank A. R. Wildes for numerous discussions. The work was supported by the EU Graphene Flagship project. M.E.Z. acknowledges support from the ANR, France, Grant No. ANR-19-CE30-0040. This work was supported by the Czech Science Foundation, Project No. 22-21974S. Z.S. was supported by the ERC-CZ program (project LL2101) of the Ministry of Education Youth and Sports (MEYS) and used large infrastructure from Project Reg. No. CZ.02.1.01/0.0/0.0/15_003/0000444 financed by the EFRR. The authors also acknowledge the support of the LNCMI-CNRS in Grenoble, a member of the European Magnetic Field Laboratory (EMFL).

[1] J.-G. Park, Opportunities and challenges of 2D magnetic van der Waals materials: Magnetic graphene? J. Phys.: Condens. Matter **28**, 301001 (2016).

[2] R. Samal, G. Sanyal, B. Chakraborty, and C. S. Rout, Two-dimensional transition metal phosphorous trichalcogenides (MPX_3): A review on emerging trends, current state and future perspectives, J. Mater. Chem. A **9**, 2560 (2021).

[3] B. L. Chittari, Y. Park, D. Lee, M. Han, A. H. MacDonald, E. Hwang, and J. Jung, Electronic and magnetic properties of single-layer MPX_3 metal phosphorous trichalcogenides, Phys. Rev. B **94**, 184428 (2016).

[4] B. Taylor, J. Steger, A. Wold, and E. Kostiner, Preparation and properties of iron phosphorus triselenide $FePSe_3$, Inorg. Chem. **13**, 2719 (1974).

[5] G. Le Flem, R. Brec, G. Ouvard, A. Louisy, and P. Segransan, Magnetic interactions in the layer compounds MPX_3 (M = Mn, Fe, Ni; X = S, Se), J. Phys. Chem. Solids **43**, 455 (1982).

[6] H. Li, S. Ruan, and Y.-J. Zeng, Intrinsic van der Waals magnetic materials from bulk to the 2D limit: New frontiers of spintronics, Adv. Mater. **31**, 1900065 (2019).

[7] P. Ferloni and M. Scagliotti, Magnetic phase transitions in iron and nickel phosphorus trichalcogenides, Thermochim. Acta **139**, 197 (1989).

[8] A. Wiedenmann, J. Rossat-Mignod, A. Louisy, R. Brec, and J. Rouxel, Neutron diffraction study of the layered compounds $MnPSe_3$ and $FePSe_3$, Solid State Commun. **40**, 1067 (1981).

[9] K. C. Rule, G. J. McIntyre, S. J. Kennedy, and T. J. Hicks, Single-crystal and powder neutron diffraction experiments on $FePS_3$: Search for the magnetic structure, Phys. Rev. B **76**, 134402 (2007).

[10] A. R. Wildes, K. C. Rule, R. I. Bewley, M. Enderle, and T. J. Hicks, The magnon dynamics and spin exchange parameters of $FePS_3$, J. Phys.: Condens. Matter **24**, 416004 (2012).

[11] D. Lançon, H. C. Walker, E. Ressouche, B. Ouladdiaf, K. C. Rule, G. J. McIntyre, T. J. Hicks, H. M. Rønnow, and A. R. Wildes, Magnetic structure and magnon dynamics of the quasi-two-dimensional antiferromagnet $FePS_3$, Phys. Rev. B **94**, 214407 (2016).

[12] A. R. Wildes, M. E. Zhitomirsky, T. Ziman, D. Lançon, and H. C. Walker, Evidence for biquadratic exchange in the quasi-two-dimensional antiferromagnet $FePS_3$, J. Appl. Phys. **127**, 223903 (2020).

[13] T. Sekine, M. Jouanne, C. Julien, and M. Balkanski, Light-scattering study of dynamical behavior of antiferromagnetic spins in the layered magnetic semiconductor $FePS_3$, Phys. Rev. B **42**, 8382 (1990).

[14] X. Wang, K. Du, Y. Y. F. Liu, P. Hu, J. Zhang, Q. Zhang, M. H. S. Owen, X. Lu, and C. K. Gan, Raman spectroscopy of atomically thin two-dimensional magnetic iron phosphorus trisulfide ($FePS_3$) crystals, 2D Mater. **3**, 031009 (2016).

[15] A. McCreary, J. R. Simpson, T. T. Mai, R. D. McMichael, J. E. Douglas, N. Butch, C. Dennis, R. V. Aguilar, and A. R. H. Walker, Quasi-two-dimensional magnon identification in antiferromagnetic $FePS_3$ via magneto-Raman spectroscopy, Phys. Rev. B **101**, 064416 (2020).

[16] S. Liu, A. Granados del Águila, D. Bhowmick, C. K. Gan, T. Thu Ha Do, M. A. Prosnikov, D. Sedmidubský, Z. Sofer, P. C. M. Christianen, P. Sengupta, and Q. Xiong, Direct observation of magnon-phonon strong coupling in two-dimensional antiferromagnet at high magnetic fields, Phys. Rev. Lett. **127**, 097401 (2021).

[17] D. Vaclavkova, M. Palit, J. Wyzula, S. Ghosh, A. Delhomme, S. Maity, P. Kapuscinski, A. Ghosh, M. Veis, M. Grzeszczyk, C. Faugeras, M. Orlita, S. Datta, and M. Potemski, Magnon polarons in the van der Waals antiferromagnet $FePS_3$, Phys. Rev. B **104**, 134437 (2021).

[18] J. Wyzula, I. Mohelský, D. Václavková, P. Kapuscinski, M. Veis, C. Faugeras, M. Potemski, M. E. Zhitomirsky, and M. Orlita, High-angular momentum excitations in collinear antiferromagnet $FePS_3$, Nano Lett. **22**, 9741 (2022).

[19] C. Kittel, Theory of antiferromagnetic resonance, Phys. Rev. **82**, 565 (1951).

[20] F. Keffer and C. Kittel, Theory of antiferromagnetic resonance, Phys. Rev. **85**, 329 (1952).

[21] C. Kittel, *Quantum Theory of Solids* (Wiley, New York, 1987).

[22] J. Luo, S. Li, Z. Ye, R. Xu, H. Yan, J. Zhang, G. Ye, L. Chen, D. Hu, X. Teng, W. A. Smith, B. I. Yakobson, P. Dai, A. H. Nevidomskyy, R. He, and H. Zhu, Evidence for topological magnon–phonon hybridization in a 2D antiferromagnet down to the monolayer limit, Nano Lett. **23**, 2023 (2023).

[23] J. Cui, E. V. Boström, M. Ozerov, F. Wu, Q. Jiang, J.-H. Chu, C. Li, F. Liu, X. Xu, A. Rubio, and Q. Zhang, Chirality selective magnon-phonon hybridization and magnon-induced chiral phonons in a layered zigzag antiferromagnet, Nat. Commun. **14**, 3396 (2023).

[24] R. Silberglitt and J. B. Torrance, Effect of single-ion anisotropy on two-spin-wave bound state in a Heisenberg ferromagnet, Phys. Rev. B **2**, 772 (1970).

[25] K. Wierschem, Y. Kato, Y. Nishida, C. D. Batista, and P. Sengupta, Magnetic and nematic orderings in spin-1 antiferromagnets with single-ion anisotropy, Phys. Rev. B **86**, 201108(R) (2012).

[26] D. Petitgrand, A. Brun, and P. Meyer, Magnetic field dependence of spin waves and two magnon bound states in FeI_2, J. Magn. Magn. Mater. **15–18**, 381 (1980).

[27] K. Katsumata, H. Yamaguchi, M. Hagiwara, M. Tokunaga, H.-J. Mikeska, P. Goy, and M. Gross, Single-ion magnon bound states in an antiferromagnet with strong uniaxial anisotropy, Phys. Rev. B **61**, 11632 (2000).

[28] X. Bai, S.-S. Zhang, Z. Dun, H. Zhang, Q. Huang, H. Zhou, M. B. Stone, A. I. Kolesnikov, F. Ye, C. D. Batista, and M. Mourigal, Hybridized quadrupolar excitations in the spin-anisotropic frustrated magnet FeI_2, Nat. Phys. **17**, 467 (2021).

[29] R. L. Dally, A. J. R. Heng, A. Keselman, M. M. Bordelon, M. B. Stone, L. Balents, and S. D. Wilson, Three-magnon bound state in the quasi-one-dimensional antiferromagnet α-$NaMnO_2$, Phys. Rev. Lett. **124**, 197203 (2020).

[30] A. Legros, S.-S. Zhang, X. Bai, H. Zhang, Z. Dun, W. A. Phelan, C. D. Batista, M. Mourigal, and N. P. Armitage, Observation of 4- and 6-magnon bound states in the spin-anisotropic frustrated antiferromagnet FeI_2, Phys. Rev. Lett. **127**, 267201 (2021).

[31] D. Jana, P. Kapuscinski, A. Pawbake, A. Papavasileiou, Z. Sofer, I. Breslavetz, M. Orlita, M. Potemski, and C. Faugeras, In-plane anisotropy in the van der Waals antiferromagnet $FePSe_3$ probed by magneto-Raman scattering, Phys. Rev. B **108**, 144415 (2023).

[32] E. Rastelli, A. Tassi, and L. Reatto, Non-simple magnetic order for simple Hamiltonians, Physica B+C (Amsterdam) **97**, 1 (1979).

[33] A. R. Wildes, D. Lançon, M. K. Chan, F. Weickert, N. Harrison, V. Simonet, M. E. Zhitomirsky, M. V. Gvozdikova, T. Ziman, and H. M. Rønnow, High field magnetization of $FePS_3$, Phys. Rev. B **101**, 024415 (2020).

[34] A. Pawbake, T. Pelini, A. Delhomme, D. Romanin, D. Vaclavkova, G. Martinez, M. Calandra, M.-A. Measson, M. Veis, M. Potemski, M. Orlita, and C. Faugeras, High-pressure tuning of magnon-polarons in the layered antiferromagnet $FePS_3$, ACS Nano **16**, 12656 (2022).

[35] E. Rastelli and A. Tassi, Normal modes in an anisotropic antiferromagnet, Phys. Rev. B **11**, 4711 (1975).

[36] U. Balucani, V. Tognetti, and M. Pini, Kinematic consistency in anisotropic ferromagnets, J. Phys. C **12**, 5513 (1979).

[37] J. Oitmaa and C. J. Hamer, Ground-state properties and one-particle spectra for a spin-1 Heisenberg antiferromagnet from series expansions, Phys. Rev. B **77**, 224435 (2008).

[38] E. M. Wheeler, R. Coldea, E. Wawrzyńska, T. Sörgel, M. Jansen, M. M. Koza, J. Taylor, P. Adroguer, and N. Shannon, Spin dynamics of the frustrated easy-axis triangular antiferromagnet $2H$-$AgNiO_2$ explored by inelastic neutron scattering, Phys. Rev. B **79**, 104421 (2009).

[39] M. Wortis, Bound states of two spin waves in the Heisenberg ferromagnet, Phys. Rev. **132**, 85 (1963).

[40] J. Hanus, Bound states in the Heisenberg ferromagnet, Phys. Rev. Lett. **11**, 336 (1963).

[41] A. V. Chubukov, Chiral, nematic, and dimer states in quantum spin chains, Phys. Rev. B **44**, 4693(R) (1991).

[42] L. Kecke, T. Momoi, and A. Furusaki, Multimagnon bound states in the frustrated ferromagnetic one-dimensional chain, Phys. Rev. B **76**, 060407(R) (2007).

[43] Q. Zhang, M. Ozerov, E. V. Bostrm, J. Cui, N. Suri, Q. Jiang, C. Wang, F. Wu, K. Hwangbo, J.-H. Chu *et al.*, Coherent strong-coupling of terahertz magnons and phonons in a van der Waals antiferromagnetic insulator, arXiv:2108.11619.

[44] K. Okuda, K. Kurosawa, and S. Saito, High field magnetization process in $FePS_3$, in *High Field Magnetism*, edited by M. Date (North Holland, Amsterdam, 1983), pp. 55–58.

[45] K. Kurosawa, S. Saito, and Y. Yamaguchi, Neutron diffraction study on $MnPS_3$ and $FePS_3$, J. Phys. Soc. Jpn. **52**, 3919 (1983).

[46] L. Chen, X. Teng, D. Hu, F. Ye, G. E. Granroth, M. Yi, J.-H. Chung, R. J. Birgeneau, and P. Dai, Thermal evolution of spin excitations in honeycomb Ising antiferromagnetic $FePSe_3$, arXiv:2402.16983.